




Magnetic domain structure of epitaxial Gd films grown on W(110)Patrick Härtl ^{1,*}, Markus Leisegang ¹ and Matthias Bode ^{1,2}¹*Physikalisches Institut, Experimentelle Physik II, Universität Würzburg, Am Hubland, 97074 Würzburg, Germany*²*Wilhelm Conrad Röntgen-Center for Complex Material Systems (RCCM), Universität Würzburg, Am Hubland, 97074 Würzburg, Germany*

(Received 16 February 2022; revised 3 May 2022; accepted 10 May 2022; published 26 May 2022)

We present a detailed real-space spin-polarized scanning tunneling microscopy (SP-STM) study of the magnetic domain structure of Gd(0001) films epitaxially grown on W(110). To find optimal preparation conditions, the influence of the substrate temperature during deposition and of the postgrowth annealing temperature was investigated. Our results show that the lowest density of surface defects, such as step edges as well as screw and edge dislocations, is obtained for room-temperature deposition and subsequent annealing at 900 K. SP-STM data reveal small-size magnetic domains at lower annealing temperatures, evidently caused by pinning at grain boundaries and other crystalline defects. The coverage-dependent magnetic domain structure of optimally prepared Gd films was systematically investigated. For low coverage up to about 80 atomic layers (AL), we observe μm -size domains separated by domain walls which are oriented approximately along the $[1\bar{1}0]$ direction of the underlying W substrate. Above a critical film thickness $\Theta_{\text{crit}} \approx (100 \pm 20)$ AL, we identify stripe domains, indicative of a spin reorientation transition from in plane to out of plane. In agreement with existing models, the periodicity of the stripe domains increases the further the coverage exceeds Θ_{crit} . While the orientation of the stripe domains is homogeneous over large distances just above Θ_{crit} , we find a characteristic zigzag pattern at $\Theta \gtrsim 200$ AL and irregular stripe domains beyond 500 AL. Intermediate minima and maxima of the magnetic signal indicate the nucleation of branching domains. The results are discussed in terms of various contributions to the total magnetic energy, such as the magnetocrystalline, magnetostatic, and magnetoelastic energy density.

DOI: [10.1103/PhysRevB.105.174431](https://doi.org/10.1103/PhysRevB.105.174431)**I. INTRODUCTION**

The functionality of numerous technical devices relies on magnetic thin films. For example, they are used as positioning or speed sensors [1] and magnetic hard disk drives still represent the backbone of present mass data-storage applications [2]. The progress we have witnessed in the past decades required a thorough understanding of the physical processes which determine the properties of thin magnetic films, such as the saturation magnetization, the remanent magnetization, or the coercive field. In polycrystalline or granular materials, however, the intricate interplay between structural defects and magnetic domain walls impedes a clear identification of the underlying physical processes.

In this context, thin films grown epitaxially on single crystalline and highly pure substrates offer an invaluable playground to study the impact structural properties have on the magnetization behavior. Surface-adapted [3] and surface-sensitive [4] magnetic measurement techniques allow for a detailed understanding, especially if combined with microscopic imaging methods [5–10]. In particular, thin $3d$ transition-metal (TM) films deposited on the surfaces of noble or refractory metals were intensively studied. For example, these investigations provided consistent pictures of the onset of long-range order at island coalescence [11,12], of film thickness-dependent spin reorientation transitions [13–15],

and of the development of a uniaxial anisotropy on vicinal, highly stepped surfaces [16,17]. Furthermore, the capability of imaging magnetic surfaces with atomic spin resolution by spin-polarized scanning tunneling microscopy (SP-STM) [5] led to the discovery of highly complex spin structures, such as ferro- and antiferromagnetic spin cycloids [18,19] and two-dimensional magnetic skyrmions [20].

In contrast, very little is known about the magnetic domain structures of thin rare-earth-metal (REM) films. Recent real-space imaging studies are limited to Dy [21–23], Tb [24], and Nd [25] films deposited on W(110). Given the important role REMs play in permanent magnets and considering their fundamentally different magnetic coupling mechanism, which relies on the Ruderman-Kittel-Kasuya-Yosida (RKKY) interaction rather than the direct exchange at work in $3d$ TMs, this is very surprising. Potentially, this lack of high-spatial-resolution magnetic domain studies is related to the extreme reactivity of REMs, which not only imposes high standards on the cleanliness of the substrate and the evaporant, but also on the vacuum conditions during deposition [26,27]. Gadolinium (Gd) is considered to be the prototype ferromagnet among the lanthanides with localized magnetic moments. Bulk Gd is ferromagnetic with a Curie temperature $T_C = 293$ K [28]. Since its $4f$ shell is half filled, Hund coupling results in a magnetic $4f$ spin moment of $7\mu_B$ and a vanishing orbital moment with an almost spherical charge distribution. Accordingly, in comparison with the other REMs, the magnetocrystalline anisotropy energy density of bulk Gd is very low.

*Corresponding author: patrick.haertl@physik.uni-wuerzburg.de

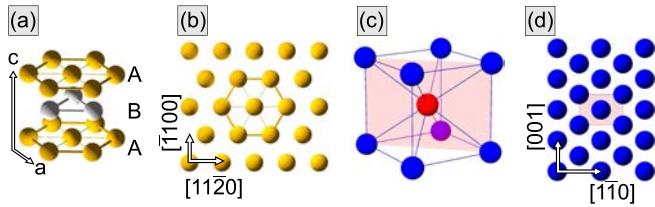


FIG. 1. (a) The hexagonal close-packed A/B/A stacking model for gadolinium including the a and c axes. (b) The corresponding (0001) plane of this structure with the crystallographic $[1\bar{1}20]$ and $[\bar{1}100]$ directions. (c) Body-centered-cubic unit cell of tungsten with (d) the atomic structure of the (110) plane and the $[1\bar{1}0]$ and $[001]$ directions.

Gd crystallizes in the hexagonal close-packed (hcp) crystal structure with an alternating sequence of A/B/A layers; see Figs. 1(a) and 1(b). With a c/a ratio of 1.59, the hcp lattice structure of bulk Gd deviates somewhat from the ideal value, $c/a = 1.633$. This causes an anisotropic dipole-dipole interaction which, if considered in isolation, would result in a magnetization pointing along the c axis. In combination with the above-mentioned small magnetocrystalline anisotropy, it results in an easy axis which—at low temperatures relevant for this study—is rotated by about 30° away from the c axis [29].

The magnetic properties of Gd thin films epitaxially grown on the (110) surface of refractory body-centered-cubic (bcc) W single crystals have been investigated in numerous studies. The epitaxial growth relation between these two materials is $\text{Gd}(0001) \parallel \text{W}(110)$ and $\text{Gd}[1\bar{1}20] \parallel \text{W}[1\bar{1}0]$ [30]. It was recognized at an early stage that both the film thickness [31] and the annealing temperature [32,33] significantly affect the magnetic properties. The observed enhancement of the ac susceptibility χ_{ac} was interpreted in terms of misfit dislocations which are annealed at elevated temperature, whereby the temperature required to optimize the height and width of the χ_{ac} peak increased with increasing film thickness [32].

Susceptibility measurements also resulted in the identification of a spin reorientation transition (SRT) from in-plane to out-of-plane magnetized stripe domains for $\Theta \geq \Theta_{\text{crit}} = 40 \text{ nm}$ [34–36]. This transition was explained with the competition of two energy contributions, i.e., the stray field or magnetostatic energy and the uniaxial magnetocrystalline anisotropy energy. Whereas the former dominates for thin films, the latter becomes more relevant for thick films and leads to a rotation of the magnetization towards the c axis, i.e., perpendicular to the surface plane of $\text{Gd}(0001)/\text{W}(110)$ [35,36].

A lively discussion developed around the question of whether or not the topmost surface layer of $\text{Gd}(0001)$ films on $\text{W}(110)$ possesses extraordinary magnetic properties, such as an enhanced surface Curie temperature [37,38] or an imperfect or even antiferromagnetic coupling to the bulk [39,40]. In this context, a spin-split d_{z^2} -like surface state of $\text{Gd}(0001)$ was intensively investigated [41–45], essentially rebutting any surface-related magnetic anomaly. The well-defined spin polarization of the occupied majority and the unoccupied minority part of this surface state was later used to establish

the spectroscopic mode of spin-polarized scanning tunneling microscopy (SP-STM) [46,47].

Here we report on a systematic SP-STM investigation of the film thickness-dependent magnetic domain structure of $\text{Gd}(0001)$ films epitaxially grown on $\text{W}(110)$. To identify optimal growth conditions, both the substrate temperature during Gd deposition and the postdeposition annealing temperature were modified. We find that room-temperature deposition results in the smoothest films with the lowest density of surface defects, such as step edges, screw, and edge dislocations. Spin-resolved measurements clearly show that annealing Gd films at a temperature of 600 K is insufficient to release stacking faults from the as-grown films, resulting in relatively small domains, probably due to domain wall pinning. Only upon annealing to 900 K were large domains with straight domain walls observed. A coverage-dependent SP-STM study of $\text{Gd}/\text{W}(110)$ in the coverage range between 20 and 600 AL finds a spin-reorientation transition (SRT) from in plane to out of plane at a critical coverage $\Theta_{\text{crit}} \approx (100 \pm 20) \text{ AL}$, in excellent agreement with earlier findings based on susceptibility measurements [35,36]. Stripe domains are imaged for $\Theta > \Theta_{\text{crit}}$. The high spatial resolution of SP-STM allows for an investigation of the stripe periodicity. While we find that the magnetic stripe domains are homogeneously tilted by either $+30^\circ$ or -30° with respect to the $\text{W}[001]$ direction just above Θ_{crit} , a zigzag pattern with an alternating stripe orientation is found between 200 and 375 AL. In the same coverage regime, we find evidence for the formation of branching domains. At even higher Gd coverage, irregular stripe domains are found. The observed magnetic domain structures are discussed in terms of competing effects, i.e., the magnetocrystalline, magnetostatic, and magnetoelastic contributions to the total energy.

II. EXPERIMENTAL SETUP AND PROCEDURES

The experiments were performed in a two-chamber ultrahigh vacuum (UHV) system with a base pressure $p \leq 5 \times 10^{-11} \text{ mbar}$. A preparation chamber facilitates tip and sample preparation by electron-beam heating to temperatures well above 2300 K. Variable leak valves allow for the dosing of high-purity gases. The $\text{W}(110)$ single crystal was initially cleaned in an oxygen atmosphere by a two-step-flashing procedure with consecutive low-temperature ($T_{\text{sample}} \approx 1200 \text{ K}$) and high-temperature ($T_{\text{sample}} \gtrsim 2200 \text{ K}$) flashes [48]. Flash temperatures were measured with an optical pyrometer (Iron Ultimex UX-20P) at an emissivity $\epsilon = 0.33$ and an estimated accuracy of $\pm 100 \text{ K}$. The cleanliness of the substrate was confirmed by a sharp low-energy electron diffraction (LEED) pattern with a low background intensity, as will be shown further below, and by scanning tunneling microscopy (STM).

Distilled Gd lumps (MaTeck, purity 99.99%) were melted in a Mo crucible and deposited by electron-beam evaporation. The *absolute* deposition rate is determined to (19.8 ± 3.7) atomic layers (AL) per minute [49], where the error margin corresponds to a statistical uncertainty due to the limited scan range of our STM images. Therefore, we expect a much lower *relative* error between samples with different Gd coverage, as they are achieved by a simple scaling of the

deposition time. During deposition and LEED experiments, the sample was clamped to a manipulator which can either be cooled by liquid nitrogen, resulting in a sample temperature $T_{\text{sample}} \gtrsim 120$ K, or heated by a filament ($T_{\text{sample}} \lesssim 1000$ K). On the manipulator, the sample temperature is measured by a thermocouple attached to one side of the sample slot. Comparison of temperature readings taken with the optical pyrometer and the thermocouple in the temperature range between 590 and 890 K agree within ≈ 50 K.

Upon preparation, the samples were transferred into the STM chamber. This chamber includes a cryostat cooled with liquid helium which houses a home-built low-temperature STM. It is operated at a base temperature $T_{\text{STM}} \approx 4.5$ K. Measurements were performed with electrochemically etched W tips. All images were taken in the constant-current mode with the bias voltage U_{bias} applied to the sample. Tunneling dI/dU spectra and maps were obtained by modulating the bias voltage at a frequency $f_{\text{mod}} = 5.309$ kHz, i.e., well above the cutoff frequency of the feedback loop, and detecting the resulting amplitude of the current modulation with a lock-in amplifier. Typical amplitudes of the bias voltage modulation were $U_{\text{mod}} = 10$ mV.

For magnetically sensitive spin-polarized STM measurements, the tip was dipped several nanometers into the Gd surface or gently pulsed at voltages $U_{\text{bias}} \geq \pm 4$ V. As stated in more detail in Sec. III C, this preparation procedure reliably resulted in probe tips which gave a strong tunneling magnetoresistance (TMR) contrast in differential conductivity dI/dU images, especially around $U_{\text{bias}} \approx -700$ mV. Furthermore, it has the advantage that it comes with a much lower experimental effort than the preparation of thin film tips described in earlier publications [5], which required a high-temperature treatment and subsequent film deposition and annealing. At the same time, however, it has the disadvantage that the tip magnetization direction is probably not aligned along the in-plane or out-of-plane direction, but canted relative to the sample surface. For thin film tips, in contrast, the magnetization direction can be predicted with reasonable confidence [5] and verified by scanning suitable test samples; for an example, see Fig. S3 in Ref. [50]. Our preference for a swift magnetic tip preparation technique rather than a much slower method with a more reliable quantization axis is a consequence of the focus of this study, which is on the systematic investigation of a broad variety of preparation parameters, such as the substrate temperature during film deposition, the postgrowth annealing temperature, and the Gd film thickness. The sheer number of experimental runs excluded alternative tip preparation procedures. As a result, the easy axis of the domain or the magnetic orientation of domain walls cannot be deduced directly from our SP-STM results. Instead, our interpretation also relies on comparison with published results obtained with spatially averaging experimental techniques [30,35] and the comparison with domain pattern observed on sample systems other than Gd. Furthermore, the rather large amount of magnetic material in Fe-coated tips often led to a modification of the Gd domain patterns, as observed previously with other sample systems [51]. Our experience shows that magnetic tips prepared by dipping into the Gd film are much less invasive, probably because the effective amount of material is much smaller.

For better visibility of our STM data, the z signal recorded in the topographic constant-current image was augmented by its derivative with respect to the fast scan direction, dz/dx . This image processing suggests to the observer a topography image that is illuminated by an invisible light source from the left. Depending on the maximal corrugation, the exact mixing ratio of z and dz/dx varies for different images of this study. As a result, the color code cannot be directly interpreted as height information. Wherever necessary, line profiles will be presented to allow for a quantitative assessment. Details of the STM image processing can be found in the Supplemental Material [49].

III. RESULTS

A. Structural properties

Deposition temperature. In the literature, the effect of the W(110) substrate temperature on the Gd film quality has been discussed to some extent. While the majority of studies [26,26,32,44–46,52,53] deposit at about 300 K, some report on enhanced [30,33,39] or reduced temperatures [54]. In order to identify the optimal growth conditions for later magnetic domain studies, we deposited Gd films with a thickness of 80 AL onto the W(110) substrate held at various temperatures. Figure 2 shows STM overviews of samples grown at (a) $T_{\text{dep}} = 120$, (b) 300, and (c) 590 K. Upon film growth, all samples were postannealed on an electron-beam stage at $T_{\text{ann}} \geq 900$ K for five minutes. Height profiles measured along the black transparent lines marked in Figs. 2(a)–2(c) are presented in Figs. 2(d)–2(f), respectively.

The STM topography image of the sample grown at a reduced substrate temperature [Fig. 2(a)] is dominated by numerous short step edges which often converge under an acute angle with neighboring step edges, thereby forming a zigzag pattern of V-shaped single-atomic step edges with double-screw dislocations at the joints, exemplary marked by green arrows. The typical length of these step edges is several-tens up to a few-hundred nanometers and the density of the double-screw dislocations amounts to about (172 ± 13) per μm^2 [55]. Occasionally, two single-atomic step edges emerge and terminate at the same location and run almost in parallel, thereby forming an isolated pair which closely resembles a double step edge. An example is marked by a red dashed circle. These two features, i.e., step edges with a height in close agreement with a single-atomic ($h_{\text{sa}} = 289$ pm) and a double-atomic ($h_{\text{da}} = 578$ pm) step edge, can also be recognized in the line section presented in Fig. 2(d) as sharp transitions. Furthermore, numerous pointlike indentations (pink dashed circle) with a density of about (341 ± 18) per μm^2 , and smoothed-out step edges (gray dashed line) can be recognized, whose origin will be explained later on. We would like to note that a few sharply delimited holes with an apparent depth of about (140 ± 20) pm can be recognized, one of which is marked by a brown dashed circle. It has been shown in previous studies that these holes are caused by the local adsorption of hydrogen, resulting in the quenching of the d_{z^2} -like Gd(0001) surface state [26]. These holes cover less than 0.1% of the total surface area, thereby corroborating the excellent cleanliness of the surface.

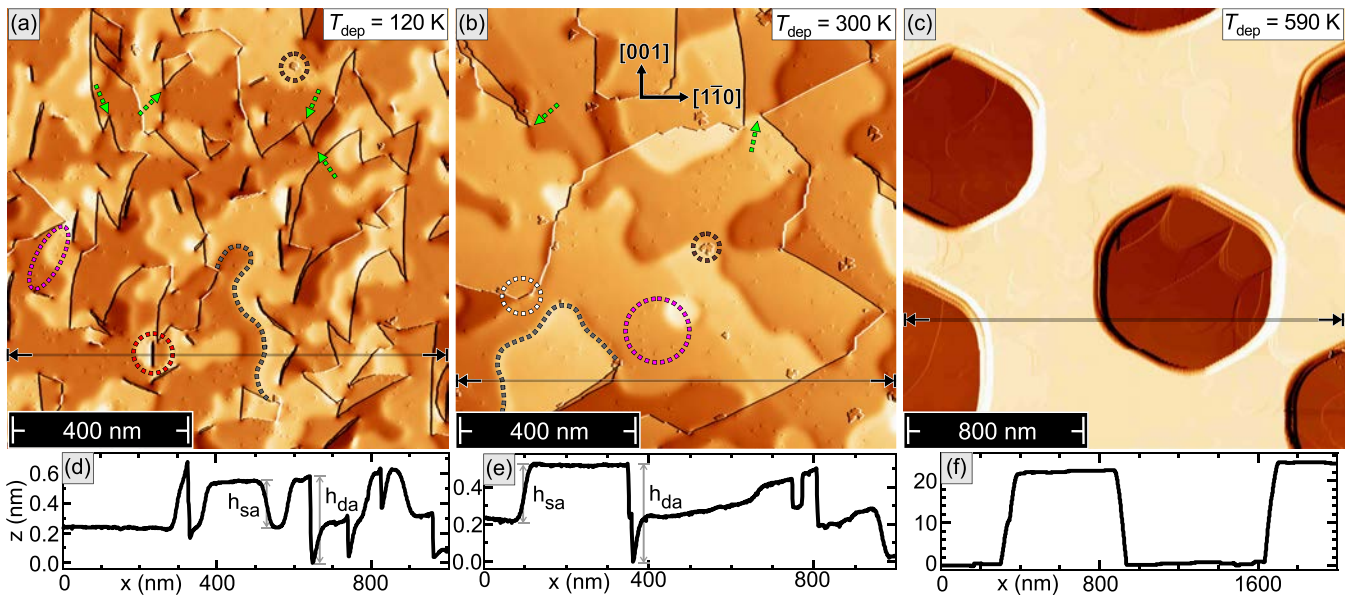


FIG. 2. STM topographic images for 80-AL-thick Gd films on W(110) deposited at substrate temperatures of (a) $T_{\text{dep}} = 120$, (b) 300, and (c) 590 K. Upon deposition, the films were annealed at $T_{\text{ann}} \geq 900$ K for five minutes. The height profiles below each panel were taken along the respective lines. Scan parameters: $U_{\text{bias}} = -700$ mV and $I_{\text{set}} = 1$ nA.

The sample prepared at room temperature [Fig. 2(b)] exhibits a much lower density of these structural features and, therefore, the overall surface morphology appears much smoother. For example, the density of the V-shaped single-step edges is reduced to about (31 ± 6) per μm^2 , i.e., a reduction of about 82% as compared to the low-temperature grown film presented in Fig. 2(a). A similar reduction is also identified for the pointlike indentations (pink dashed circle) to about (202 ± 14) per μm^2 , which is about 41% less than for the cold evaporation. The density of smoothed step edges (indicated by a gray dashed line) is also reduced by a similar percentage. The height profile presented in Fig. 2(e) confirms these observations.

The Gd film grown at $T_{\text{dep}} = 590$ K shows a completely different surface morphology; see Fig. 2(c). Here we find large hexagonal vacancy islands with depths $h \geq 20$ nm and typical side lengths of about 400 nm [see, also, the line profile in Fig. 2(f)]. Obviously, the film thickness is no longer homogeneous but at the edge to island formation, in general agreement with similar observations made for thinner films [33].

These results indicate that the optimal substrate temperature for obtaining homogeneous Gd films with a minimal density of structural defects is ≈ 300 K. In contrast, elevated or lowered temperatures result in surface textures with more structural defects, which potentially act as pinning centers for magnetic domain walls and are, therefore, unsuitable for imaging the intrinsic domain structure of Gd/W(110) films. A similar behavior with respect to the annealing temperature will be presented in Sec. III C below.

Growth. Figure 3 summarizes the main processes that are important to understand the structural features of Gd(0001) films grown on W(110). All samples were deposited at room temperature and postannealed at $T_{\text{anneal}} \geq 900$ K for 5 min. Figure 3(a) shows an overview of the terrace-and-step structure of a 20 AL film. The overgrown step edges of the

underlying W substrate can clearly be identified. The zoom-in image reveals that the terraces are not perfectly flat, but exhibit trenches which are about (30 ± 5) pm deep. One example is marked by a cyan circle in Fig. 3(b). Furthermore, numerous pointlike indentations (pink circle) can be recognized.

When increasing the film thickness to 30 AL [Fig. 3(c)], the film texture changes considerably, as the trenches become deeper (up to 170–240 pm). Furthermore, they are more asymmetric and—in some segments—have even converted into full-fledged step edges. Some positions where the transition from an asymmetric trench into a step edge is observed are marked by green dashed circles in the higher magnification image presented in Fig. 3(d). This transition not only results in a screw dislocation, but also in the appearance of smoothed-out step edges, which appear as white bumps in Fig. 3(d). At an even higher film thickness of 40 AL [see Fig. 3(e)], the surface morphology is dominated by smoothed steps and double-screw dislocations, some of which are marked by blue dashed circles in the zoom-in in Fig. 3(f). These features have completely replaced the trenches observed at lower coverage, which no longer can be found.

Overall, the thickness-dependent changes observed in Figs. 3(a)–3(e) for Gd/W(110) show a close resemblance to earlier results of Dy films grown on W(110) reported by Krause *et al.* [21]. In this report, it was shown by atomic resolution data that pointlike indentations similar to those we observed in Figs. 2(a) and 3(b) are caused by edge dislocations, i.e., an additional semi-infinite plane which releases misfit-related strain. Furthermore, Krause and co-authors proposed a general model [21], which is reproduced in Figs. 3(g)–3(j), that describes the evolution of the rare-earth-metal (REM) film morphology on bcc(110) surfaces. The first atomic layer of heavy REMs epitaxially grown on W(110) single crystals reveals a heavily distorted hexagonal lattice [30,56]. The nucleation of A- and B-stacked islands,

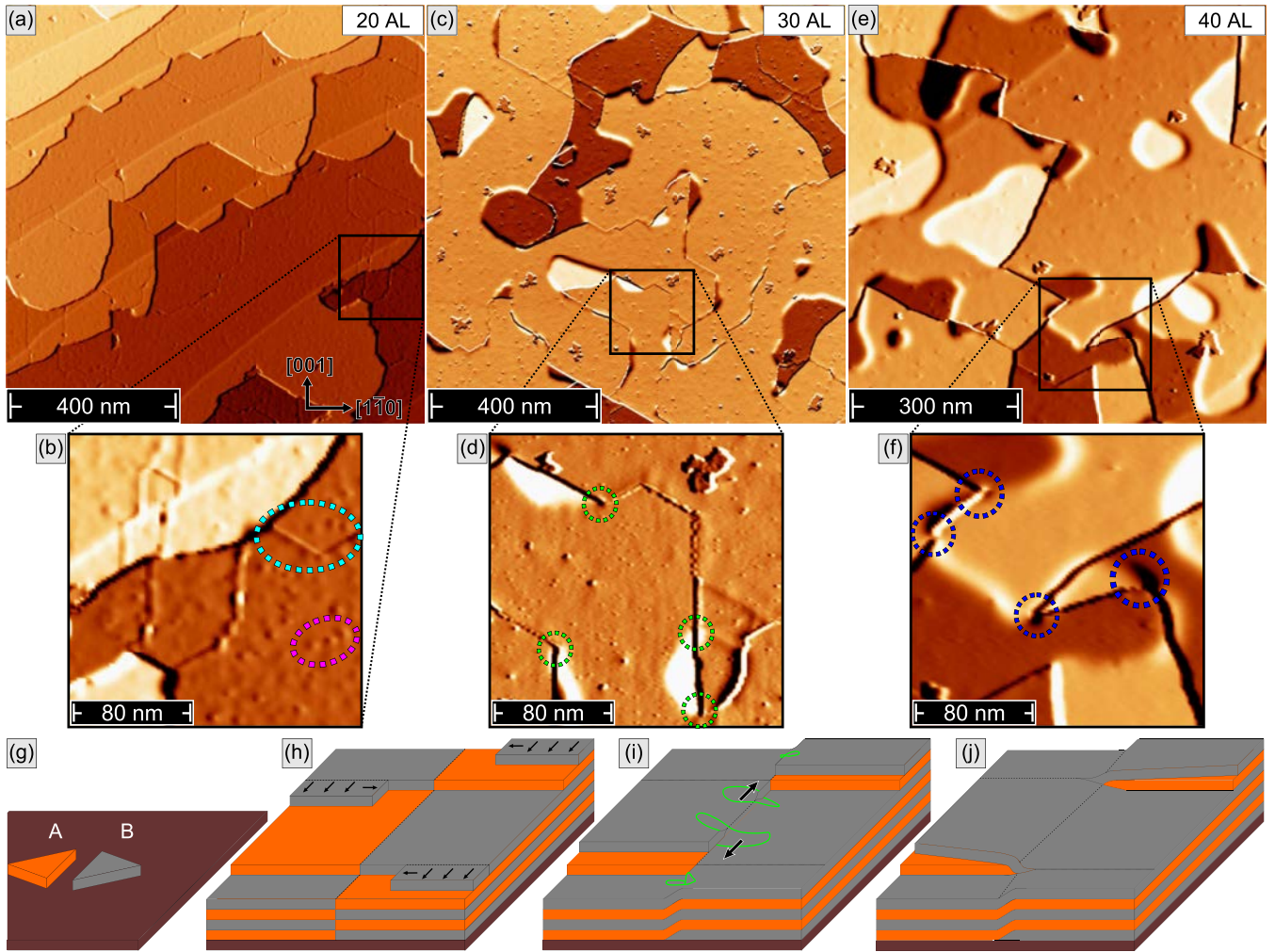


FIG. 3. (a), (c), (e) STM topography images of the thickness-dependent surface structures of Gd films on W(110) for (a) 20, (b) 30, and (c) 40 AL. (b), (d), (f) Zoomed-in data to highlight characteristic structural defects. Scan parameters $U_{\text{bias}} = -700$ mV, $I_{\text{set}} = 1$ nA. (g)–(j) Model explaining the formation of structural stacking faults and their relaxation via glide dislocations. Initially, (g) A- or B-stacked islands nucleate, which (h) lead to structural grain boundaries as the film closes (arrows indicate film growth direction). (i) The resulting film stress is relaxed via the formation of screw dislocations, which move with increasing film thickness (indicated by arrows) and eventually (j) form characteristic double-screw dislocations.

schematically represented in Fig. 3(g), starts with the second atomic layer [44]. These islands grow to patches which maintain their respective stacking order, i.e., A/B/A or B/A/B, even after coalescence when a continuous film is formed at relatively low coverage. As indicated by the differently colored surface layers in Fig. 3(h), however, the film is not translation invariant at the grain boundary between two of these patches, resulting in structural domain boundaries which we observe as trenches in Figs. 3(a) and 3(b).

Since the energy associated with the grain boundary increases with increasing film thickness, relaxation processes set in at a critical thickness; see Fig. 3(i). They lead to so-called partial screw dislocations, which shift differently stacked patches by half a lattice constant along the c axis, i.e., perpendicular to the film plane, and result in a film with continuous A- and B-stacked layers. However, this process is accompanied by a significant surface buckling, which in our data appears as smoothed-out step edges; cf. Figs. 2(a), 2(b) and 3(d). Obviously, for Gd films on W(110), this process

starts at a coverage somewhere between 20 and 30 AL. As indicated by black arrows in Fig. 3(i), these partial screw dislocations move with increasing film thickness until an adjacent pair merges; see Fig. 3(j). In this case, their fate depends on the relative orientation of their respective Burgers vectors, $\vec{b} = \pm[0001]$. If the two Burgers vectors point in the same direction, a double-screw dislocation with its characteristic V-shaped step structure will emerge at the sample surface; cf. Figs. 3(e) and 3(f) for a 40 AL film. In contrast, if the two Burgers vectors have opposite signs, the partial screw dislocations will annihilate and form an extended smoothed step edge. This appearance remains qualitatively unchanged up to the thickest Gd films studied here, i.e., 600 AL.

B. Electronic properties

Figure 4 summarizes spin-averaged STM measurements for a 200-AL-thick Gd(0001)/W(110) film taken with an unpolarized W tip (see Supplemental Material in Ref. [49]).

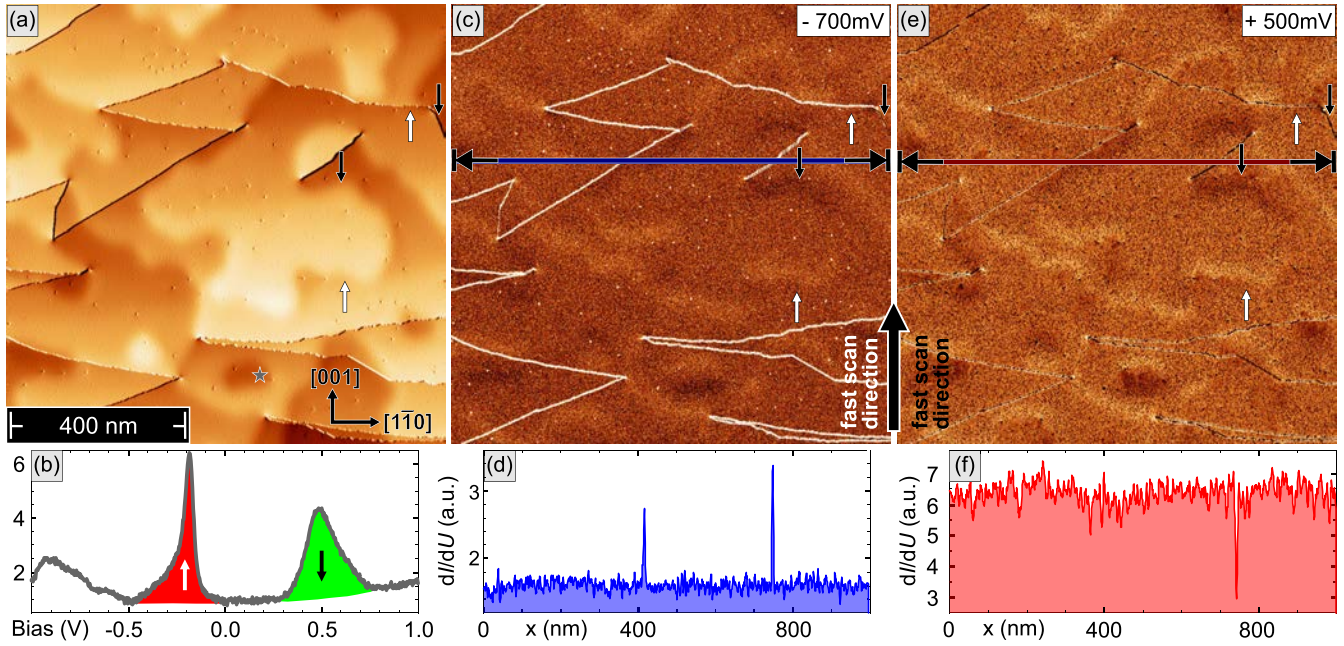


FIG. 4. Spin-averaged STM measurements performed on a 200-Å-thick Gd(0001) film on W(110) with an unpolarized W tip. (a) The topography image shows a surface with few defects and the characteristic V-shaped double-screw dislocations. (b) Tunneling dI/dU spectrum measured at the position marked by a gray star in (a). The occupied majority (red) and the unoccupied minority (green) part of the $5d_{z^2}$ -like surface state can clearly be recognized as peaks. (c) dI/dU map of the same area shown in (a) measured at a bias voltage $U_{\text{bias}} = -700$ mV, giving access to the density of states at the energy of the unoccupied part of the Gd(0001) surface state. (d) Smoothed line profile of the dI/dU signal taken along the blue-transparent line in (c). (e), (f) Same as (c), (d), but now measured at $U_{\text{bias}} = +500$ mV. Stabilization current: $I_{\text{set}} = 1$ nA.

The film was prepared by room-temperature deposition and postgrowth annealing at $T_{\text{anneal}} \geq 900$ K for 5 min. In agreement with the data presented so far, the STM topography image shown in Fig. 4(a) exhibits a surface morphology with characteristic double-screw dislocations and smoothed step edges. At the location marked with a gray star in Fig. 4(a), a dI/dU point spectrum was taken, which is plotted in Fig. 4(b). It shows two pronounced peaks which originate from the well-known exchange-split $5d_{z^2}$ -like surface states of Gd(0001). The occupied majority part appears at a binding energy of $eU = -190$ meV, whereas the empty minority part is observed at $eU = +480$ meV, highlighted in red and green in Fig. 4(b), respectively. These values are in good agreement with the binding energies reported in earlier scanning tunneling spectroscopy (STS) studies [45,46,57] and in a combined angle-resolved photoemission (PE) and inverse PE study by Weschke *et al.* [42].

Figures 4(c) and 4(e) shows dI/dU maps which were simultaneously obtained at bias voltages $U_{\text{bias}} = -700$ mV and $U_{\text{bias}} = +500$ mV, respectively. As evidenced by the respective slightly smoothed line profiles, presented in Figs. 4(d) and 4(f) below, in both cases the dI/dU signal strength shows a relatively small variation, indicating an almost constant density of states (DOS) if measured with a nonmagnetic probe tip. The only exceptions are a weak modulation which occurs on length scales of about 100 nm and more narrow dips/peaks. Correlation with the topography image in Fig. 4(a) reveals that these variations of the dI/dU signal are not related to the local electronic properties of the Gd film, but instead are caused by the finite response time of the feedback circuit. A

thick arrow between Figs. 4(c) and 4(e) indicates the fast scan direction of these data sets. Obviously, when scanning the tip over smoothed step edges or step edges, such as those marked by arrows in Fig. 4(a), the tip needs to be retracted whenever the sample height increases (upward slope, white arrows) and extended if the sample height decreases (downward slope, black arrows). Due to the finite response time of the feedback circuit, this results in a subtle increase or decrease of the tunneling current I , respectively. Comparison of the topography in Fig. 4(a) with the dI/dU maps presented in Figs. 4(c) and 4(e) reveals that this variation of the I results in a dI/dU signal which is enhanced at every upward slope and reduced at downward slopes. The backward scan (opposite fast scan direction, not shown here) exhibits the opposite trend. Therefore, we can conclude that the spin-averaged density of states of the surface of Gd films grown on W(110) as measured with nonmagnetic probe tips is essentially homogeneous. As we will see below, this changes if magnetic probe tips are used and enables the imaging of magnetic domains.

C. Magnetic properties

Postgrowth annealing temperature. It has been shown in numerous reports that the annealing temperature significantly affects the magnetic properties of Gd(0001) films grown on W(110) substrates [32–34,36]. For example, 50-nm-thick films showed a reduced low-temperature coercivity if annealed at $T_{\text{ann}} = 570$ K, an effect which was attributed to the annealing of defects [36]. It was argued that “the domain wall mobility is enhanced with improving crystal quality,” thereby

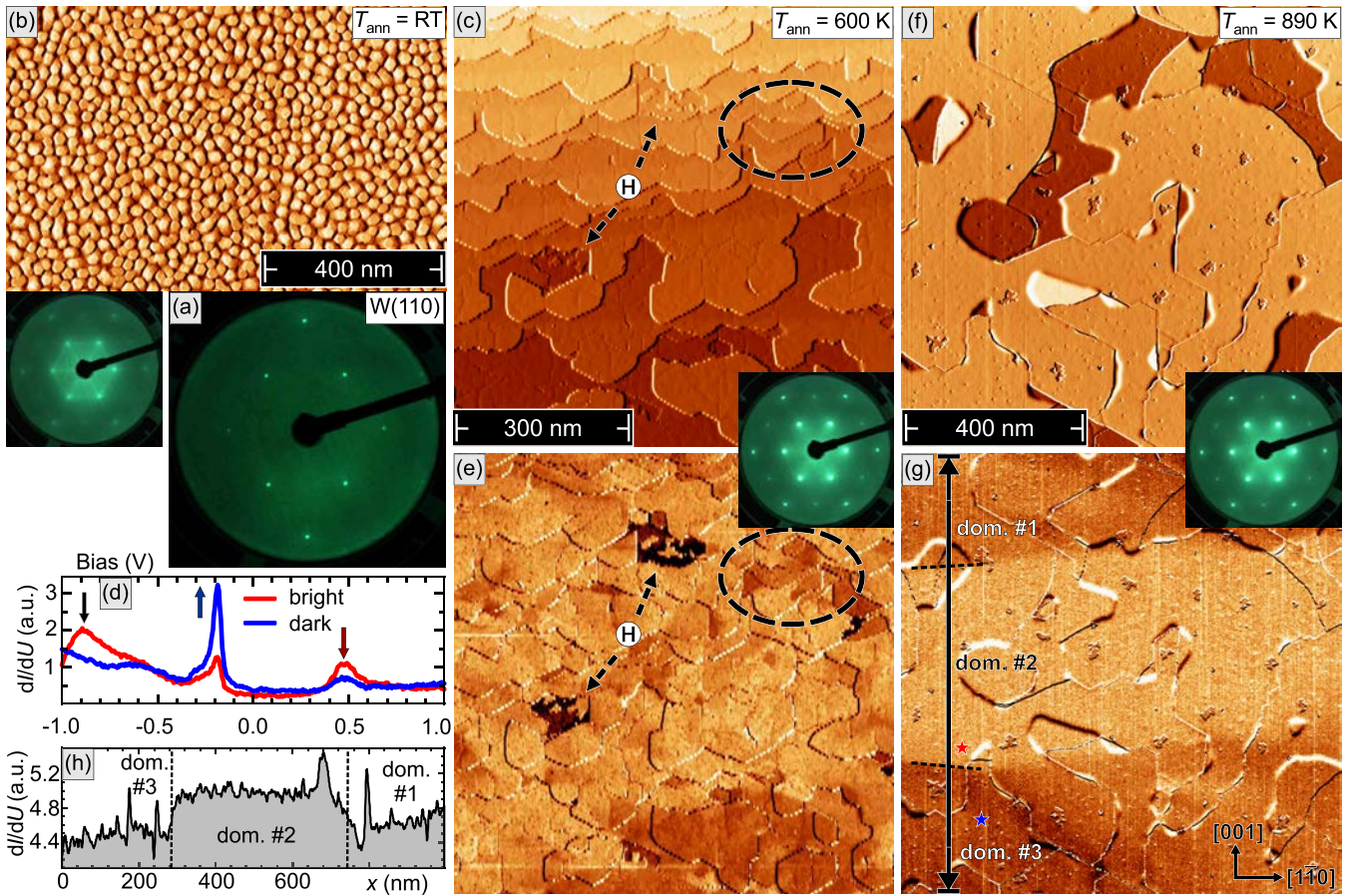


FIG. 5. (a) LEED diffraction figure of the clean W(110) crystal. (b) Overview scan of a 30-Å-thick Gd(0001) film grown on W(110) at room temperature without postannealing. (c) Topography of a similar film as (b), but postannealed at $T_{\text{ann}} = 600$ K. (d) Typical dI/dU point spectra measured with a magnetically sensitive Gd/W tip. (e) Magnetically sensitive dI/dU signal of the same sample surface presented in (c). Note that the dark contrast is not of magnetic origin, but caused by the local adsorption of hydrogen (marked H). (f) Topography and (g) magnetically sensitive dI/dU signal of 30 Å Gd(0001)/W(110) upon annealing at $T_{\text{ann}} = 890$ K. (h) Line section of the dI/dU signal measured along the arrows in (g). The insets show the evolution of the LEED pattern with increasing annealing temperatures. LEED parameters: $T_{\text{LEED}} = 110$ K, $E_{\text{LEED}} = 133$ eV. STM parameters: $U_{\text{bias}} = -700$ mV, $I_{\text{set}} = 1$ nA.

resulting “in a reduction of the coercive field” [36]. However, it has also been shown that too high annealing temperatures may result in discontinuous films [32,33,58,59].

In order to appropriately evaluate the effects the annealing temperature has on both the surface morphology and the magnetic domain structure, we exemplarily performed a combined LEED and SP-STM study of 30 Å Gd/W(110); see Fig. 5. Figure 5(a) displays the LEED pattern of clean W(110). As shown in the STM image of Fig. 5(b), Gd deposition without any further annealing results in a very rough surface with numerous hexagon-shaped islands with a typical diameter of 20 nm and several nanometer deep trenches. Similar to earlier reports [32], the corresponding LEED pattern, which is shown as an inset in Fig. 5(b), exhibits diffuse refraction spots, most likely resulting from poor long-range order.

Figure 5(c) shows an STM image of a Gd film which was postannealed at $T_{\text{ann}} = 600$ K for 15 minutes. The surface topography is comparable to the data presented in Fig. 3(a) further above. We recognize a decent terrace-and-step growth without any screw dislocations. However, the terraces are not flat, but exhibit a large number of line defects, as already discussed in Sec. III A, indicating a high density of grain

boundaries between differently stacked patches of the film. The LEED pattern displayed in the inset shows sharp refraction spots, thereby confirming a much improved crystallinity as compared to the as-grown film presented in Fig. 5(b).

Typical dI/dU spectra obtained with a spin-polarized Gd/W tip on two locations of a Gd/W(110) film are shown in Fig. 5(d). The locations were chosen somewhat arbitrarily such that the spectra show maximum contrast. We recognize two spectra which are very similar qualitatively, i.e., if solely judged on the basis of the general spectral shape and the peak positions, but which—at least at some bias voltages—differ quite significantly in terms of the dI/dU signal strength. In close accordance with the spin polarization of Gd(0001) determined by spin-resolved inverse photoemission spectroscopy [60] and previously published SP-STs results obtained with Fe-coated probe tips [46,47], we find a contrast reversal between the occupied majority [marked \uparrow in Fig. 5(d)] and the unoccupied minority part (\downarrow) which takes place at a bias voltage $U_{\text{bias}} \approx +350$ mV. However, with the Gd tips employed here, we find an additional contrast reversal in the occupied states at $U_{\text{bias}} \approx -500$ mV. It appears to be related to a peak which is located at around $U \approx -900$ mV; see black arrow

in Fig. 5(d). We tentatively attribute this feature in our STS data to a bundle of Gd bands which originate from hybridizing majority $5d$ - and $6s$ -derived states and disperse in the ΓK direction of the surface Brillouin zone [61]. As described in Figs. 8 and 9 of Ref. [61], these bands can be found in the energy range between 0.5 and 1.0 eV below the Fermi level, exhibit a very flat dispersion, and, therefore, are expected to result in an appreciable majority DOS in the surface layer. We would like to note that the bias voltage range just below this peak, especially around $U \approx -700$ mV, turned out to be particularly suited for spin-resolved dI/dU mapping experiments with Gd/W tips, as the magnetic contrast was most reliable and rather stable.

The spin-dependent contrasts identified in Fig. 5(d) can be utilized to map the magnetic domain structure of the Gd(0001) surface. Figure 5(e) presents a spin-resolved dI/dU map which was obtained with a magnetically sensitive Gd/W tip simultaneously with the topographic image of Fig. 5(c). The contrast variation here is caused by spin-polarized tunneling and reflects the domain structure of the film [62]. The magnetic domains visible in Fig. 5(e) are quite irregular, e.g., in the region marked by hatched black ellipses, and often form tiny patches. We speculate that this domain structure is the result of the pinning of magnetic domain walls at structural defects, such as step edges or structural grain boundaries.

As evidenced by the data presented in Figs. 5(f) and 5(g), annealing of the films profoundly changes the magnetic domain structure of Gd films on W(110). Again, a 30-AL-thick Gd film was deposited at room temperature, but the post-annealing temperature is increased to $T_{\text{ann}} \approx 890$ K for 15 min. In comparison to Fig. 5(c), the topographic STM image shown in Fig. 5(f) reveals a much improved surface quality with a strongly reduced density of step edges and structural grain boundaries. At the same time, the LEED pattern (inset) is basically undistinguishable from the one presented in Fig. 5(c), indicating that the short-range crystalline order on length scales of the coherence length of low-energy electrons (≈ 100 nm) remains unchanged. Although this annealing results in the formation of double-screw dislocations, as described before in Fig. 3, the magnetic domain structure changes considerably, as can be seen in the spin-sensitive dI/dU map shown in Fig. 5(g). On a $1 \times 1 \mu\text{m}^2$ scan range, we recognize only three magnetic domains, marked as dom. #1 through dom. #3, which are separated by domain walls (highlighted by hatched lines) roughly oriented along the $W[1\bar{1}0]$ direction. A line profile of the dI/dU signal along the arrow across the three domains is plotted in Fig. 5(h). In contrast to the essentially flat data taken with nonmagnetic tips [cf. Figs. 4(d) and 4(f)], the line profile presented here features two contrast levels. While a lower dI/dU signal is recorded at domains #1 and #3, a higher signal is measured for domain #2. Obviously, the reduced density and different kind of structural defects upon annealing to 890 K leads to a strong reduction of the pinning potential for magnetic domain walls. As a result, the film is able to adapt a more uniform domain structure.

Although we are not able to unambiguously determine whether the magnetic domain structures imaged in Fig. 5(g) represent an in-plane or an out-of-plane contrast, we interpret the strongly anisotropic course of the domains walls along the $W[1\bar{1}0]$ direction as evidence for a magnetization which is

oriented in plane along this direction. Thereby, the magneto-static energy associated with head-to-head or tail-to-tail spin configurations can be avoided. Unfortunately, a comparison of these data with previous experimental results is in many cases complicated by an insufficient documentation of the scattering geometry. One of the few exceptions is the study of Weller *et al.*, [30] where it is explicitly stated that their spin-polarized low-energy electron diffraction (SPLEED) experiments are essentially sensitive to a magnetization along the $W[1\bar{1}0]$ direction, in agreement with our hypothesis above.

Film thickness-dependent domain structure. We have performed an extensive SP-STM investigation of the thickness-dependent magnetic domain structures of Gd films grown on W(110). As described before, the films were deposited at room temperature and subsequently annealed at $T_{\text{anneal}} \geq 900$ K for five minutes on an electron-beam heating stage. We would like to note that a large part of the data presented in Figs. 6 and 7 has been obtained in a relatively short experimental run with the identical tip for which we can exclude even minor tip changes; see Ref. [63]. The complete set of data consists of 12 different coverages. The first, low-coverage part of this study is presented in Fig. 6. The six data sets displayed are arranged in two rows divided by a horizontal black line. Each row is subdivided into three columns which show the STM topography in the top and the corresponding, simultaneously measured magnetic dI/dU map in the bottom image. All images show a scanned area of $1 \times 1 \mu\text{m}^2$.

Starting at 20 AL, the Gd film thickness is still below the onset where relaxation processes set in; cf. Fig. 3(h). Correspondingly, the topographic image in Fig. 6(a) exhibits flat terraces separated by single-atomic step edges. On the terraces, numerous trenches can be recognized which are characteristic for the structural grain boundaries between differently stacked patches. Yet, as can be seen in the magnetically sensitive dI/dU map of Fig. 6(b), due to the high annealing temperature their density is sufficiently reduced to allow for large domains. Domain walls are roughly oriented along the $W[1\bar{1}0]$ direction. Within individual domains, a weak spatial variation of the dI/dU signal can be recognized. For example, the bright domain which covers more than the upper half of the image exhibits areas with a slightly enhanced or reduced dI/dU signal. Comparison of the structural and magnetic data displayed in Figs. 6(a) and 6(b), respectively, reveals that the modification of the magnetic dI/dU signal correlates with the orientation of the structural grain boundaries which separate differently stacked patches of the film; cf. Fig. 3(c). Due to the hexagonal symmetry of the Gd surface layer, the structural grain boundaries come in three orientations, marked by blue, red, and green arrows in Fig. 6(b). We speculate that the grain boundaries are accompanied by an additional in-plane anisotropy term which causes the magnetization to locally deviate from the $W[1\bar{1}0]$ direction. This deviation leads to an improved or poorer alignment with the tip magnetization, resulting in an enhanced or reduced dI/dU signal due to the TMR effect, respectively. In Fig. 6(b), regions with grain boundaries oriented along $Gd[1\bar{1}00] \parallel W[001]$ (blue arrows) appear brighter, whereas a darker contrast is observed in regions where they are oriented along $Gd[\bar{1}010]$ (green) or $Gd[01\bar{1}0]$ (red). It appears that these dislocation-induced deviations of the magnetization are

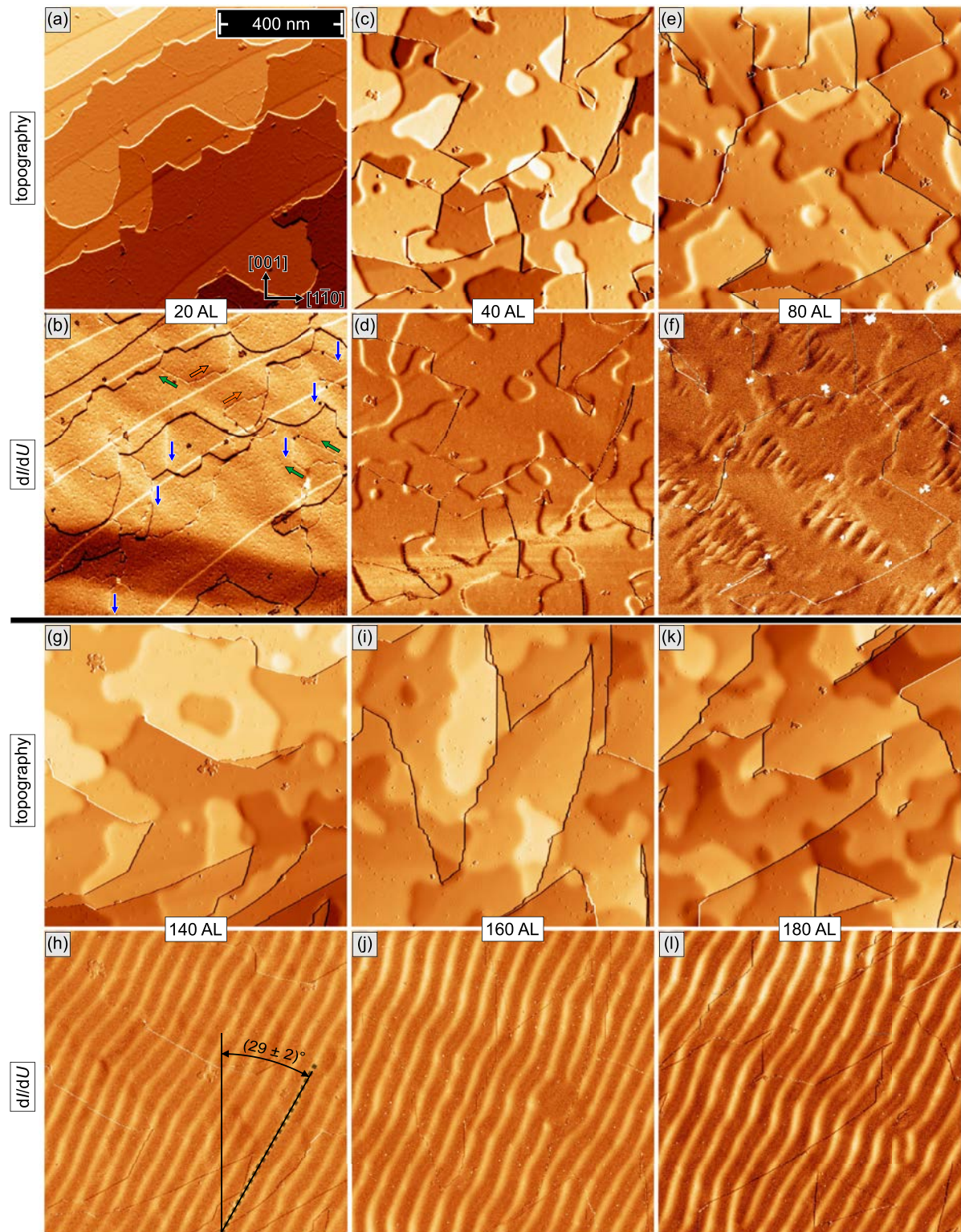


FIG. 6. First part of a coverage-dependent series of topographic images (top) and the simultaneously measured magnetically sensitive dI/dU maps (bottom) of Gd(0001) films grown on a W(110) substrate (continued in Fig. 7). While a few large domains with domain walls running along the W[110] direction can be recognized at low coverage, i.e., for (a), (b) 20 AL and (c), (d) 40 AL, stripe domains which are tilted by an angle $\alpha = (25 \dots 30)^\circ$ against the W[001] direction can be found between (g), (h) 140 AL and (k), (l) 180 AL. A transitional state between the two regimes is shown in (e) and (f). Scan parameters: $U_{\text{bias}} = -700$ mV, $I_{\text{set}} = 1$ nA.

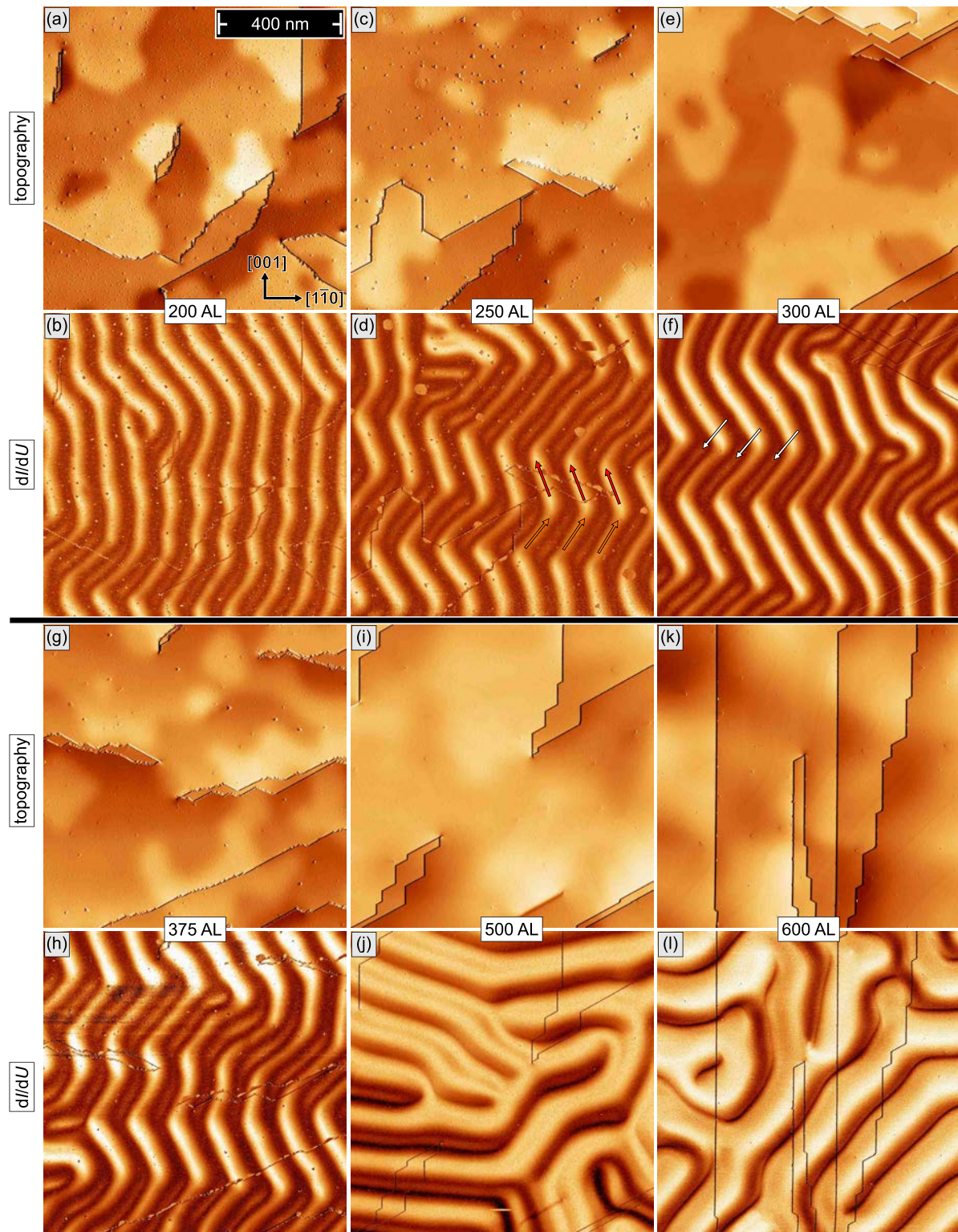


FIG. 7. Second part of a coverage-dependent series of Gd(0001) films grown on a W(110) substrate (continued from Fig. 6). At coverages between (a), (b) 200 AL and (g), (h) 375 AL, the orientation of these stripe domains periodically switches between positive and negative tilt angles, resulting in an apparent zigzaglike domain pattern. For even thicker films between (i), (j) 500 AL and (k), (l) 600 AL, a wormlike magnetic domain pattern with even larger periodicities is found. Scan parameters: $U_{\text{bias}} = -700$ mV and $I_{\text{set}} = 1$ nA.

also responsible for some, if not all, fluctuations of the domain wall orientation.

Inspection of the STM image of a 40 AL film, displayed in Fig. 6(c), reveals that the structure of the film has changed

considerably. The presence of numerous double-screw dislocations and smooth step edges evidences that the film thickness is above the threshold for the relaxation; cf. Fig. 3(i). Nevertheless, the domain structure represented in Fig. 6(d) is

essentially the same as for the 20 AL film of Figs. 6(a) and 6(b), as it still shows a few extended domains with domain walls along the $W[1\bar{1}0]$ direction.

When increasing the Gd coverage further to 80 AL up to 180 AL, the structural properties of the surface as imaged by STM remain largely unchanged; see Figs. 6(e), 6(g), 6(i), and 6(k). In either case, the topography of the surface is dominated by double-screw dislocations, smoothed step edges, and numerous pointlike defects, indicating the presence of edge dislocations. Yet, the magnetic domain structure changes considerably. For a Gd coverage of 80 AL [Fig. 6(f)], we observe several triangle- or lens-shaped areas which exhibit a stripe pattern, whereas the surrounding surface still shows a homogeneous dI/dU signal. The lateral size of the striped areas typically amounts to a few-hundred nanometers. When performing several experimental runs, we found this inhomogeneous surface magnetic structure at nominal coverages of (100 ± 20) AL. We speculate that the variation originates from slight fluctuations of the growth parameters which are beyond our control.

At even higher coverage, between 140 and 180 AL, shown in Figs. 6(h), 6(j) and 6(l), pronounced periodic stripes cover the entire sample surface. As exemplarily indicated in Fig. 6(h), these stripes are initially tilted by about $(29 \pm 2)^\circ$ with respect to the $[001]$ direction of the W substrate. We would like to note that negative tilt angles also occurred, as exemplarily shown in Fig. S4(b) of the Supplemental Material [49]. Already a superficial inspection suggests that the periodicity of these stripes increases with coverage. Furthermore, an increasing tendency towards orientational deviations from straight stripes becomes manifest. The data presented in Figs. 6(j) and 6(l) suggest that the dark stripes are broader than the bright stripes. Close inspection reveals that for these 160 and 180 AL thick films, a faint intermediate intensity is visible within the dark regions. As will be pointed out below, these effects become more pronounced for even thicker films.

These impressions are further substantiated by the data taken on Gd films with higher coverages, which are presented in Fig. 7. For Gd coverages between 200 AL [Figs. 7(a) and 7(b)] and 375 AL [Figs. 7(g) and 7(h)], the stripe orientation more or less periodically switches between positive and negative tilt angles, resulting in an apparent zigzaglike domain pattern. Furthermore, the brightness of the stripes, which are tilted by positive and negative angles, becomes increasingly different. These data clearly reveal that the magnetic dI/dU signal for some stripes no longer oscillates between a minimal and maximal value, but exhibits intermediate maxima. Faint bright lines, three of which are marked by white arrows in Fig. 7(f), become visible within the dark segments of the stripes which are rotated in the clockwise direction. These observations will be discussed in Sec. IV in detail.

Finally, for very thick films with a Gd coverage of 500 AL [Fig. 7(i)] or even 600 AL [Fig. 7(k)], the surface topography becomes more and more smooth with fewer and fewer double-screw dislocations, step edges, and edge dislocations. This change in film structure is accompanied by a magnetic domain structure where the domains and domain walls no longer follow certain crystallographic directions, but instead wind quite irregular around one another; see Figs. 7(j) and 7(k). Nevertheless, in close similarity to the dark segments

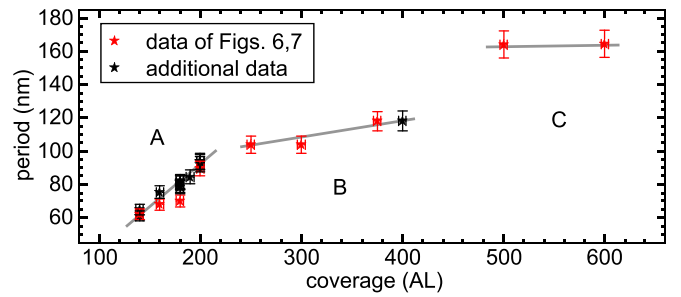


FIG. 8. Periodicity of the stripe domains as extracted from the data of Figs. 6 and 7 (red) and other SP-STM data not presented here (black). Gray lines serve as guides to the eye only. Three thickness ranges can be distinguished: (A) Between 140 and 200 AL, the periodicity increase linearly with Gd film thickness. (B) The periodicity increase levels off for $200 \leq \Theta \leq 400$ AL. (C) Another increase occurs for $400 < \Theta < 500$ AL.

observed for the clockwise-rotated stripes in the magnetically sensitive dI/dU maps of Figs. 7(b), 7(d), 7(f), and 7(h), the stripe pattern displays intermediate minima and maxima of the dI/dU signal in the bright and dark stripes, respectively.

Figure 8 summarizes the periodicities of the stripe domains extracted from Figs. 6 and 7 for Gd film thicknesses between 140 and 500 AL. We can recognize three coverage ranges, labeled A–C in Fig. 8. A linear increase is obtained in A, where the periodicity increases from (62 ± 3) nm at a 140 AL up to (91 ± 5) nm for a 200 AL thick Gd film. For even thicker Gd films, i.e., in the thickness range B of $200 \leq \Theta \leq 400$ AL, the periodicity increase seems to level off until another increase occurs towards C for $400 < \Theta < 500$ AL.

IV. DISCUSSION

The data presented in Figs. 6 and 7 can be explained qualitatively by the subtle interplay between the exchange energy, the magnetostatic energy related to the stray field, and magnetocrystalline contributions to the anisotropy. For Gd/W(110), these magnetic properties are—in comparison to bulk Gd—strongly modified by the presence of substantial epitaxial strain. For thin films up to about 60 AL, we find rather large domains; cf. Figs. 5(g), 6(b), and 6(d). SP-STM images with a scan range of $1 \times 1 \mu\text{m}^2$ typically show 1–2 domain walls only, roughly oriented along the $W[1\bar{1}0]$ direction.

As sketched in Fig. 9(a), this observation is consistent with films magnetized along this in-plane axis. It appears that—even though the easy axis of bulk Gd is tilted by 30° from the c axis—a perpendicular or canted magnetization relative to the sample plane is energetically unfavorable for thin films. This could either be caused by (i) the relatively large magnetostatic energy associated with any significant out-of-plane magnetization or (ii) by the uniaxial strain of the hexagonal Gd(0001) lattice due to epitaxial growth on the rectangular W(110) unit cell (see Fig. 1) which might modify the magnetocrystalline anisotropy energy density. Also a combination of the two effects cannot be excluded.

As the film thickness exceeds a critical value $\Theta_{\text{crit}} \approx (100 \pm 20)$ AL, a spin-reorientation transition (SRT) from in plane to out of plane is observed. While we are unable to

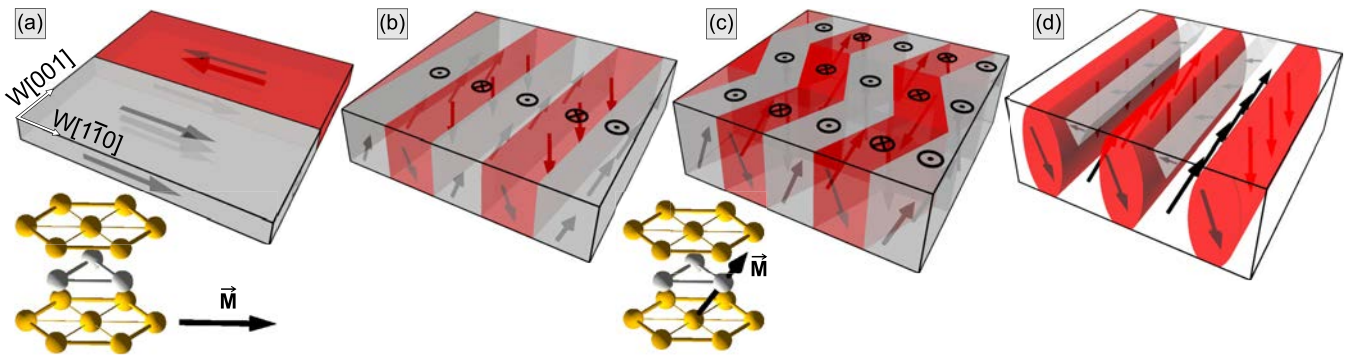


FIG. 9. Schematic representation of the thickness-dependent magnetic domain structure of Gd(0001) films grown on W(110). (a) For thin films, $\Theta > \Theta_{\text{crit}} \approx (100 \pm 20)$ AL, we find large domains with an *in-plane* easy axis oriented along $\text{Gd}[1\bar{1}20] \parallel \text{W}[1\bar{1}0]$, as indicated by a black arrow in the model of the hcp crystal structure. (b) Just above Θ_{crit} , we find tilted stripe domains, consistent with a magnetization along the $\text{Gd}[20\bar{2}3]$ direction. (c) Around 300 AL, the stripe domains form a zigzag pattern. (d) At $\Theta \geq 500$ AL, branching domains form.

identify the exact physical origin of the SRT in Gd/W(110), it is obvious that at this coverage, it becomes energetically unfavorable to align the magnetization with the film plane. If the magnetostatic energy was responsible for the in-plane magnetization [scenario (i)], the energy penalty related to the film's magnetocrystalline anisotropy overcompensates this effect for coverages $\Theta > \Theta_{\text{crit}}$. Likewise, for scenario (ii), it might be possible that the epitaxial strain relaxes to an extent unsuitable to maintain a magnetization along the in-plane axis. Upon rotation of the easy axis to out of plane, the Gd film forms stripe domains which result in a flux-closure configuration between adjacent domains and thereby reduce the sample's stray field. Stripe domains in perpendicularly magnetized thin films have been frequently observed and intensively discussed in the literature. They originate from the competition between an exchange interaction, which favors a parallel orientation of the spins, and the magnetostatic energy associated to the stray field, which can be minimized by the formation of antiparallel domains.

Particular attention was paid to the properties of stripe domains in the vicinity of a spin-reorientation transition (SRT) where the easy axis of the magnetization rotates from out of plane to in plane, or vice versa. It has generally been observed on *3d* transition-metal films with a thickness of a few atomic layers only [15,64,65] that the periodicity of the out-of-plane magnetized stripe domains decreases as one approaches the critical thickness Θ_{crit} of the SRT. Our results presented in Fig. 8 are in qualitative agreement with these results. However, in ultrathin film systems—irrespective of whether the SRT occurs from out of plane at low film thickness to in plane for thick films, or vice versa—the stripe density usually increases *exponentially* as one approaches the SRT [15,66]. In contrast, for Gd films on W(110), we find a stripe periodicity which increases *linearly* with film thickness from just above $\Theta_{\text{crit}} \approx (100 \pm 20)$ AL up to about 200 AL; cf. Fig. 8.

An analogous SRT with a critical film thickness of 27 nm and a linearly increasing stripe width has been found for FePd films [67]. The different behavior was assigned to the fact that the FePd films were much thicker than the ultrathin films mentioned above. While the spins in ultrathin films can be considered as rigidly tightened together in the vertical direction by the exchange interaction, this is not necessarily the

case for much thicker films. As a result, the magnetization component normal to the film plane, m_z , can vary with the distance from the interface [67]. Although we are not able to present a conclusive picture of how the experimentally observed domain periodicities can be explained, we speculate that the major qualitative changes of the magnetic pattern from stripe domains to zigzag stripe domains and branching domains might also be responsible for the reduced slope of the periodicity increase for Gd films with $\Theta > 200$ AL as well as for the further increase at $400 < \Theta < 500$ AL.

Interestingly, when reaching the critical film thickness $\Theta_{\text{crit}} = (100 \pm 20)$ AL, we could image indications for an inhomogeneous nucleation of stripe domains; cf. Fig. 6(f). Although we cannot strictly exclude that the weak stray field of the Gd/W tip influences these nucleation processes [51,68], our data are in good qualitative agreement with earlier photoemission electron microscopy (PEEM) experiments, where the local melting of stripe domains was observed, thereby giving rise to paramagnetic patches [66].

At coverages $\Theta > \Theta_{\text{crit}}$, the data of Figs. 6(h), 6(j) 6(l) and Figs. 7(b), 7(d) 7(f), 7(h) showed stripe domains which were not oriented along a low-index in-plane axis of the W(110) substrate, but rotated within the film plane by about $\pm 30^\circ$ with respect to the W[001] direction. At the same time, we know from the literature that the bulk easy magnetization direction of Gd is tilted by 30° relative to the *c* axis. Both conditions can be approximately fulfilled simultaneously by a magnetization which is, for example, oriented along the $\text{Gd}[20\bar{2}3]$ direction, indicated by a black arrow in the inset of Fig. 9(b).

This vector includes an angle of $\approx 36^\circ$ with respect to the *c* axis and its projection onto the (0001) surface is tilted by 30° to the W[001] and the $\text{Gd}[\bar{1}100]$ direction. The resulting magnetic domain structure, which is schematically represented in the sketch of Fig. 9(b), is in very good agreement with the conclusions drawn by Berger and co-workers based on susceptibility measurements [34–36]. Also, the critical film thickness $\Theta_{\text{crit}} \approx (100 \pm 20)$ AL identified by us agrees reasonably well with the value of 40 nm determined by Berger and co-workers, which corresponds to 138 AL [35,36].

As the film thickness is increased beyond approximately 200 AL, several interesting effects can be observed. First, the stripes are no longer straight. Instead of extended areas with

uniformly oriented domains, we find stripes whose orientation frequently changes between $+30^\circ$ and -30° , thereby forming a zigzag pattern with a typical distance between turning points of several-hundred nanometers. This zigzag pattern may be related to magnetoelastic interactions caused by the uniaxial strain associated to the growth of Gd on a W(110) crystal surface. Since the crystallographic symmetry of the W(110) surface imposes two mirror lines, i.e., the [001] and the $[1\bar{1}0]$ axes, any situation where the domain and domain wall orientation uniformly deviate from these axes would result in a net magnetoelastic strain which is incompatible with the “elastic environment”; see Sec. 3.3.1 in Ref. [69]. By forming magnetic domains which more or less periodically switch their orientation between $+30^\circ$ and -30° , any global strain away from the above-mentioned axes is avoided.

Second, the magnetic contrast observed for stripe domains which are rotated by $+30^\circ$ and -30° with respect to the W[001] direction is strikingly different; cf. Figs. 7(d), 7(f) and 7(h). In these data sets—all measured with the same magnetic tip [63]—the (anti)clockwise rotated domains appear much darker (brighter). Since purely out-of-plane domains would degenerate with respect to the rotational sense, we conclude that a significant in-plane component also exists. We speculate that this canted magnetization is the result of a significant magnetocrystalline contribution. As discussed in the context of Fig. 9(b), we expect that the in-plane component of the magnetization is oriented along the $[20\bar{2}3]$ or equivalent directions, such that the moments are along the easy axis of bulk Gd and, at the same time, aligned with the stripes domains. The schematic representation of the zigzag domain structure is presented in Fig. 9(c).

Third, the magnetic dI/dU signal of some domains of Gd films with a thickness between 250 and 375 AL no longer oscillates between a minimal and maximal value, as observed for thinner films just above the SRT, but exhibits intermediate maxima; cf. Figs. 7(d), 7(f) and 7(h). This finding may be associated with the formation of branching domains, as originally proposed by Lifshitz [70]. The general concept of branching domains is that “a progressive domain refinement towards the surface by iterated generations of domains” results in a “gain in closure energy”; see Sec. 3.7.5 in Ref. [69]. We interpret the appearance of the intermediate maximum as the first set of branching domains. A potential domain structure with in-plane closure domains is sketched in Fig. 9(d).

We would like to note, however, that the intermediate maxima could initially only be observed in regions where the darker, clockwise-rotated domains appear. No indication could be found in the anticlockwise-rotated stripe domains. We can only speculate about the reason for this asymmetry. One explanation would be that (i) branching domains exclusively exist for one stripe orientation, though we were not able to identify a simple explanation of how this directional selectivity might come about. Another explanation is (ii) related to the fact that the Gd/W tip we are using is known to exhibit a significant in-plane component. As we will show by data taken with different tips below, the branching domain increases the magnetic dI/dU signal in some regions, but has no significant effect in another region. Finally, for very thick Gd films, we observe winding stripe domains which are no longer aligned along a preferred direction. Especially in Fig. 7(j), branching

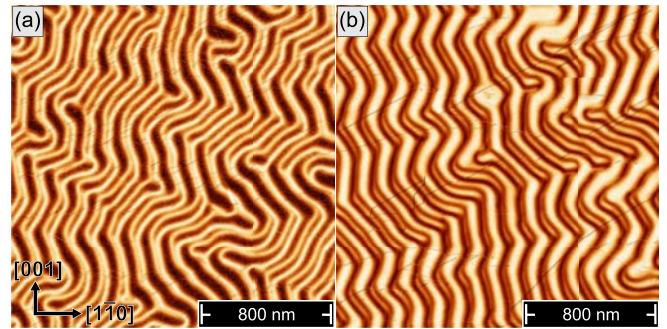


FIG. 10. Two magnetically sensitive dI/dU maps (scan size: $2 \times 2 \mu\text{m}^2$ each) measured on the same 400 AL Gd/W(110) with different Gd/W tips prepared by poking into the Gd film. The data provide strong evidence that—depending on the tip’s quantization axis—some branching domains may remain undetected (see text for details). Scan parameters: $U_{\text{bias}} = -700$ mV and $I_{\text{set}} = 1$ nA.

domains can be identified. Interestingly, this now includes both dark and bright irregular stripe domains, which clearly present weaker and rather narrow bright and dark intermediate dI/dU signals, respectively. This observation suggests that the above-mentioned absence of intermediate maxima along some stripe direction in thinner films was indeed caused by a particular tip magnetization direction unsuitable for resolving these closure domains.

As further evidence for this hypothesis, we present the data of Fig. 10 which were obtained on the same 400 AL Gd film. As described in Sec. II, the W tip was initially prepared by poking the tip into the Gd film. This Gd/W tip was then used to measure the magnetically sensitive dI/dU map presented in Fig. 10(a). Afterwards, the tip was again dipped into the Gd film to modify its quantization axis. This tip was then used to obtain the data of Fig. 10(b). Although the data were measured on the same Gd film and the observed domain structures are quite similar as far as the stripe periodicity and the general appearance are concerned, some details are strikingly different. In particular, we notice that the intermediate contrast can clearly be recognized for the entire data set of Fig. 10(a), i.e., irrespective of the stripe orientation. In contrast, the intermediate contrast can only be found for one stripe direction in Fig. 10(b). These data evidence that the apparent absence of branching domains observed in some images [cf. Figs. 7(d), 7(f) 7(h)] is not caused by their factual nonexistence, but rather by an unfavorable orientation of the tip magnetization, rendering the observation impossible.

V. SUMMARY

In this contribution, we presented a detailed spin-polarized scanning tunneling microscopy (SP-STM) study of the epitaxial Gd films grown on a W(110) surface. Our data provide high-spatial-resolution images of the magnetic domains structure of this rare-earth metal. Great care was taken to identify optimal preparation conditions which produce the lowest density of surface defects. The best results were obtained for room temperature deposition followed by subsequent annealing at 900 K. Whereas lower or higher annealing temperatures led to domain wall pinning or discontinuous films, respectively,

optimally prepared Gd films with a thickness of 30 atomic layers (AL) exhibited large in-plane magnetized domains with domain walls which are approximately oriented along the $[1\bar{1}0]$ direction of the underlying W substrate. In good agreement with earlier spatially averaging studies [34–36], we find a spin-reorientation transition (SRT) at the critical film thickness $\Theta_{\text{crit}} \approx (100 \pm 20)$ AL, where the easy axis of magnetization rotates from parallel to perpendicular to the film plane. SP-STM images taken in the thickness regime of the SRT reveal a magnetic domain structure which appears to be spatially inhomogeneous, with patches showing a stripe domain phase that coexists with paramagnetic or in-plane ferromagnetic regions. As the coverages exceed Θ_{crit} , we find stripe domains which are rotated by $\approx \pm 30^\circ$ with respect to the $W[001]$ direction. The periodicity of the stripe domains is investigated thoroughly. Furthermore, at $\Theta \gtrsim 200$ AL, we

find a magnetic domains structure which resembles a zigzag pattern. Irregular stripe domains are imaged beyond 500 AL. Our experimental data can consistently be explained by the interplay between different contributions to the total energy, i.e., the magnetocrystalline, magnetostatic, and magnetoelastic energy density.

ACKNOWLEDGMENTS

This work was supported by the DFG through SFB 1170 (Project No. A02). We also acknowledge financial support by the Deutsche Forschungsgemeinschaft (DFG, German Research Foundation) under Germany's Excellence Strategy through Würzburg-Dresden Cluster of Excellence on Complexity and Topology in Quantum Matter—ct.qmat (EXC 2147, Project No. 390858490).

-
- [1] P. Ripka and M. Janosek, *Advances in magnetic field sensors*, *IEEE Sens. J.* **10**, 1108 (2010).
- [2] W. A. Bhat, Is a data-capacity gap inevitable in big data storage? *Computer* **51**, 54 (2018).
- [3] S. D. Bader, E. R. Moog, and P. Grünberg, Magnetic hysteresis of epitaxially-deposited iron in the monolayer range: A Kerr effect experiment in surface magnetism, *J. Magn. Magn. Mater.* **53**, L295 (1986).
- [4] F. O. Schumann, R. F. Willis, and J. G. Tobin, Surface-sensitive, element-specific magnetometry with x-ray linear dichroism, *J. Vac. Sci. Techn. A* **18**, 1259 (2000).
- [5] M. Bode, Spin-polarized scanning tunnelling microscopy, *Rep. Prog. Phys.* **66**, 523 (2003).
- [6] A. Schwarz and R. Wiesendanger, Magnetic sensitive force microscopy, *Nano Today* **3**, 28 (2008).
- [7] N. Rougemaille and A. K. Schmid, Magnetic imaging with spin-polarized low-energy electron microscopy, *Eur. Phys. J. Appl. Phys.* **50**, 20101 (2010).
- [8] J. McCord, Progress in magnetic domain observation by advanced magneto-optical microscopy, *J. Phys. D: Appl. Phys.* **48**, 333001 (2015).
- [9] N. Hauptmann, J. W. Gerritsen, D. Wegner, and A. A. Khajetoorians, Sensing noncollinear magnetism at the atomic scale combining magnetic exchange and spin-polarized imaging, *Nano Lett.* **17**, 5660 (2017).
- [10] T. Kohashi, Magnetization analysis by spin-polarized scanning electron microscopy, *Scanning* **2018**, 2420747 (2018).
- [11] H. J. Elmers, J. Hauschild, H. Höche, U. Gradmann, H. Bethge, D. Heuer, and U. Köhler, Submonolayer Magnetism of Fe(110) on W(110): Finite Width Scaling of Stripes and Percolation between Islands, *Phys. Rev. Lett.* **73**, 898 (1994).
- [12] E. Mentz, A. Bauer, T. Günther, and G. Kaindl, Magnetization reversal and spin reorientation in Fe/Cu(100) ultrathin films, *Phys. Rev. B* **60**, 7379 (1999).
- [13] R. Allenspach and A. Bischof, Magnetization Direction Switching in Fe/Cu(100) Epitaxial Films: Temperature and Thickness Dependence, *Phys. Rev. Lett.* **69**, 3385 (1992).
- [14] J. Thomassen, F. May, B. Feldmann, M. Wuttig, and H. Ibach, Magnetic Live Surface Layers in Fe/Cu(100), *Phys. Rev. Lett.* **69**, 3831 (1992).
- [15] Y. Z. Wu, C. Won, A. Scholl, A. Doran, H. W. Zhao, X. F. Jin, and Z. Q. Qiu, Magnetic Stripe Domains in Coupled Magnetic Sandwiches, *Phys. Rev. Lett.* **93**, 117205 (2004).
- [16] A. Berger, U. Linke, and H. P. Oepen, Symmetry-Induced Uniaxial Anisotropy in Ultrathin Epitaxial Cobalt Films Grown on Cu(111), *Phys. Rev. Lett.* **68**, 839 (1992).
- [17] R. K. Kawakami, E. J. Escorcia-Aparicio, and Z. Q. Qiu, Symmetry-Induced Magnetic Anisotropy in Fe Films Grown on Stepped Ag(001), *Phys. Rev. Lett.* **77**, 2570 (1996).
- [18] M. Bode, M. Heide, K. von Bergmann, P. Ferriani, S. Heinze, G. Bihlmayer, A. Kubetzka, O. Pietzsch, S. Blügel, and R. Wiesendanger, Chiral magnetic order at surfaces driven by inversion asymmetry, *Nature (London)* **447**, 190 (2007).
- [19] P. Ferriani, K. von Bergmann, E. Y. Vedmedenko, S. Heinze, M. Bode, M. Heide, G. Bihlmayer, S. Blügel, and R. Wiesendanger, Atomic-Scale Spin Spiral with a Unique Rotational Sense: Mn Monolayer on W(001), *Phys. Rev. Lett.* **101**, 027201 (2008).
- [20] S. Heinze, K. von Bergmann, M. Menzel, J. Brede, A. Kubetzka, R. Wiesendanger, G. Bihlmayer, and S. Blügel, Spontaneous atomic-scale magnetic skyrmion lattice in two dimensions, *Nat. Phys.* **7**, 713 (2011).
- [21] S. Krause, L. Berbil-Bautista, T. Hänke, F. Vonau, M. Bode, and R. Wiesendanger, Consequences of line defects on the magnetic structure of high anisotropy films: Pinning centers on Dy/W(110), *Europhys. Lett.* **76**, 637 (2006).
- [22] L. Berbil-Bautista, S. Krause, M. Bode, and R. Wiesendanger, Spin-polarized scanning tunneling microscopy and spectroscopy of ferromagnetic Dy(0001)/W(110) films, *Phys. Rev. B* **76**, 064411 (2007).
- [23] L. Berbil-Bautista, S. Krause, M. Bode, A. Badía-Majós, C. de la Fuente, R. Wiesendanger, and J. I. Arnaudas, Nanoscale spin structures dominated by magnetoelastic interactions around dislocation cores as seen via spin-polarized STM, *Phys. Rev. B* **80**, 241408(R) (2009).
- [24] J. E. Prieto, G. Chen, A. K. Schmid, and J. de la Figuera, Magnetism of epitaxial Tb films on W(110) studied by spin-polarized low-energy electron microscopy, *Phys. Rev. B* **94**, 174445 (2016).

- [25] U. Kamber, A. Bergman, A. Eich, D. Iusan, M. Steinbrecher, N. Hauptmann, L. Nordström, M. I. Katsnelson, D. Wegner, O. Eriksson, and A. A. Khajetoorians, Self-induced spin glass state in elemental and crystalline neodymium, *Science* **368**, eaay6757 (2020).
- [26] M. Getzlaff, M. Bode, R. Pascal, and R. Wiesendanger, Adsorbates on Gd(0001): A combined scanning tunneling microscopy and photoemission study, *Phys. Rev. B* **59**, 8195 (1999).
- [27] D. Wegner, A. Bauer, and G. Kaindl, Effect of impurities on tamm-like lanthanide-metal surface states, *Phys. Rev. B* **76**, 113410 (2007).
- [28] K. Baberschke, M. Farle, and M. Zomack, The ferromagnetic order and the critical exponent γ of Gd monolayers and thin films on W(110), *Appl. Phys. A* **44**, 13 (1987).
- [29] W. D. Corner and B. K. Tanner, The easy direction of magnetization in gadolinium, *J. Phys. C: Solid State Phys.* **9**, 627 (1975).
- [30] D. Weller and S. F. Alvarado, Preparation of remanently ferromagnetic Gd(0001), *J. Appl. Phys.* **59**, 2908 (1986).
- [31] M. Farle, K. Baberschke, U. Stetter, A. Aspelmeier, and F. Gerhardter, Thickness-dependent Curie temperature of Gd(0001)/W(110) and its dependence on the growth conditions, *Phys. Rev. B* **47**, 11571 (1993).
- [32] U. Stetter, M. Farle, K. Baberschke, and W. G. Clark, Critical behavior of strained epitaxial Gd films: *In situ* ac-susceptibility measurements in UHV, *Phys. Rev. B* **45**, 503 (1992).
- [33] E. D. Tober, R. X. Ynzunza, C. Westphal, and C. S. Fadley, Relationship between morphology and magnetic behavior for Gd thin films on W(110), *Phys. Rev. B* **53**, 5444 (1996).
- [34] A. W. Pang, A. Berger, and H. Hopster, Magnetization behavior of thick epitaxial Gd(0001) films on W(110), *Phys. Rev. B* **50**, 6457 (1994).
- [35] A. Berger, A. W. Pang, and H. Hopster, Magnetic reorientation transition in epitaxial gd-films, *J. Magn. Magn. Mater.* **137**, L1 (1994).
- [36] A. Berger, A. W. Pang, and H. Hopster, Magnetic reorientation transition of Gd(0001)/W(110) films, *Phys. Rev. B* **52**, 1078 (1995).
- [37] D. Weller, S. F. Alvarado, W. Gudat, K. Schröder, and M. Campagna, Observation of Surface-Enhanced Magnetic Order and Magnetic Surface Reconstruction on Gd(0001), *Phys. Rev. Lett.* **54**, 1555 (1985).
- [38] H. Tang, D. Weller, T. G. Walker, J. C. Scott, C. Chappert, H. Hopster, A. W. Pang, D. S. Dessau, and D. P. Pappas, Magnetic Reconstruction of the Gd(0001) Surface, *Phys. Rev. Lett.* **71**, 444 (1993).
- [39] G. A. Mulhollan, K. Garrison, and J. L. Erskine, Surface Magnetism of Gd(0001): Evidence of Ferromagnetic Coupling to Bulk, *Phys. Rev. Lett.* **69**, 3240 (1992).
- [40] D. Li, J. Zhang, P. A. Dowben, and K. Garrison, Evidence for imperfect ferromagnetic coupling between the Gd(0001) surface and the bulk, *J. Phys.: Condens. Matter* **5**, L73 (1993).
- [41] D. Li, P. A. Dowben, J. E. Ortega, and F. J. Himpsel, Unoccupied surface electronic structure of Gd(0001), *Phys. Rev. B* **49**, 7734 (1994).
- [42] E. Weschke, C. Schüssler-Langeheine, R. Meier, A. V. Fedorov, K. Starke, F. Hübinger, and G. Kaindl, Temperature Dependence of the Exchange Splitting of the Surface State on Gd(0001): Evidence against Spin-Mixing Behavior, *Phys. Rev. Lett.* **77**, 3415 (1996).
- [43] A. V. Fedorov, T. Valla, D. J. Huang, G. Reisfeld, F. Loeb, F. Liu, and P. D. Johnson, Spin polarized photoemission studies of the Gd(0001) surface, *J. Electron Spectrosc. Relat. Phenom.* **92**, 19 (1998).
- [44] M. Getzlaff, M. Bode, S. Heinze, R. Pascal, and R. Wiesendanger, Temperature-dependent exchange splitting of the magnetic Gd(0001) surface state, *J. Magn. Magn. Mater.* **184**, 155 (1998).
- [45] M. Bode, M. Getzlaff, A. Kubetzka, R. Pascal, O. Pietzsch, and R. Wiesendanger, Temperature-Dependent Exchange Splitting of a Surface State on a Local-Moment Magnet: Tb(0001), *Phys. Rev. Lett.* **83**, 3017 (1999).
- [46] M. Bode, M. Getzlaff, and R. Wiesendanger, Spin-Polarized Vacuum Tunneling into the Exchange-Split Surface State of Gd(0001), *Phys. Rev. Lett.* **81**, 4256 (1998).
- [47] R. Wiesendanger, M. Bode, and M. Getzlaff, Vacuum-tunneling magnetoresistance: The role of spin-polarized surface states, *Appl. Phys. Lett.* **75**, 124 (1999).
- [48] Kh. Zakeri, T. R. F. Peixoto, Y. Zhang, J. Prokop, and J. Kirschner, On the preparation of clean tungsten single crystals, *Surf. Sci.* **604**, L1 (2010).
- [49] See Supplemental Material at <http://link.aps.org/supplemental/10.1103/PhysRevB.105.174431> for detailed information regarding evaluation of the deposition rate, image processing procedures, preparation of an unpolarized tip, and the verification of the stripe domains tilted in the opposite direction, and which includes the following reference: I. Horcas, R. Fernández, J. M. Gómez-Rodríguez, J. Colchero, J. Gómez-Herrero, and A. M. Baro, WSXM: A software for scanning probe microscopy and a tool for nanotechnology, *Rev. Sci. Instrum.* **78**, 013705 (2007).
- [50] M. Schmitt, P. Moras, G. Bihlmayer, R. Cotsakis, M. Vogt, J. Kemmer, A. Belabbes, P. M. Sheverdyeva, A. K. Kundu, C. Carbone, S. Blügel, and M. Bode, Indirect chiral magnetic exchange through Dzyaloshinskii-Moriya-enhanced RKKY interactions in manganese oxide chains on Ir(100), *Nat. Commun.* **10**, 2610 (2019).
- [51] A. Kubetzka, M. Bode, O. Pietzsch, and R. Wiesendanger, Spin-Polarized Scanning Tunneling Microscopy with Antiferromagnetic Probe Tips, *Phys. Rev. Lett.* **88**, 057201 (2002).
- [52] A. Aspelmeier, F. Gerhardter, and K. Baberschke, Magnetism and structure of ultrathin Gd films, *J. Magn. Magn. Mater.* **132**, 22 (1994).
- [53] U. Paschen, C. Sürgers, and H. v. Löhneysen, Magnetic properties of thin epitaxial Gd films on Nb, *Z. Phys. B* **90**, 289 (1993).
- [54] Kai Starke (private communication).
- [55] Defect densities have been determined on the basis of representative STM images with a scan range of $1 \times 1 \mu\text{m}^2$ recorded at a 1024×1024 pixel resolution. Since the number of events, N , measured within the randomly chosen sampling area follows a Poisson distribution, the error bar given is based on the standard deviation, \sqrt{N} .
- [56] J. Kołaczkiwicz and E. Bauer, The adsorption of Eu, Gd and Tb on the W (110) surface, *Surf. Sci.* **175**, 487 (1986).
- [57] D. Wegner, A. Bauer, and G. Kaindl, Magnon-broadening of exchange-split surface states on lanthanide metals, *Phys. Rev. B* **73**, 165415 (2006).
- [58] M. Farle, W. A. Lewis, and K. Baberschke, Detailed anal-

- ysis of the *in situ* magneto-optic Kerr signal of gadolinium films near the Curie temperature, *Appl. Phys. Lett.* **62**, 2728 (1993).
- [59] M. Farle and W. A. Lewis, Magnetization of thin Gd films on W(110) near the Curie temperature, *J. Appl. Phys.* **75**, 5604 (1994).
- [60] M. Donath, B. Gubanka, and F. Passek, Temperature-Dependent Spin Polarization of Magnetic Surface State at Gd(0001), *Phys. Rev. Lett.* **77**, 5138 (1996).
- [61] Ph. Kurz, G. Bihlmayer, and S. Blügel, Magnetism and electronic structure of hcp Gd and the Gd(0001) surface, *J. Phys.: Condens. Matter* **14**, 6353 (2002).
- [62] Note that the much darker patches (marked by arrows) are caused by the local adsorption of hydrogen [26]. This signal does not contain any magnetic information, but only indicates the quenching of the Gd surface state.
- [63] The identity of the tip apex was confirmed by the comparison of tunneling spectra measured on the surfaces of Figs. 7(d), 7(f), and 7(h). Since the energetic position of the d_{z^2} -like surface states remains unchanged for Gd films with a local coverage $\Theta_{\text{loc}} > 4$ AL [44], any modification of the recorded dI/dU spectra could safely be attributed to a tip change. However, the spectra measured on the sample surfaces of Figs. 7(d), 7(f), and 7(h) were virtually identical (not shown here), thereby verifying the fact that the tip apex remained unchanged during these experiments.
- [64] M. Speckmann, H. P. Oepen, and H. Ibach, Magnetic Domain Structures in Ultrathin Co/Au(111): On the Influence of Film Morphology, *Phys. Rev. Lett.* **75**, 2035 (1995).
- [65] H. P. Oepen, M. Speckmann, Y. Millev, and J. Kirschner, Unified approach to thickness-driven magnetic reorientation transitions, *Phys. Rev. B* **55**, 2752 (1997).
- [66] C. Won, Y. Z. Wu, J. Choi, W. Kim, A. Scholl, A. Doran, T. Owens, J. Wu, X. F. Jin, and Z. Q. Qiu, Magnetic stripe melting at the spin reorientation transition in Fe/Ni/Cu(001), *Phys. Rev. B* **71**, 224429 (2005).
- [67] V. Gehanno, R. Hoffmann, Y. Samson, A. Marty, and S. Auffret, In plane to out of plane magnetic reorientation transition in partially ordered FePd thin films, *Eur. Phys. J. B* **10**, 457 (1999).
- [68] A. Kubetzka, O. Pietzsch, M. Bode, and R. Wiesendanger, Spin-polarized scanning tunneling microscopy study of 360° walls in an external magnetic field, *Phys. Rev. B* **67**, 020401(R) (2003).
- [69] A. Hubert and R. Schäfer, *Magnetic Domains—The Analysis of Magnetic Microstructures* (Springer Science and Business Media, Berlin, 2008).
- [70] E. Lifschitz and E. Ruderman, On the magnetic structure of iron, in *Perspectives in Theoretical Physics: The Collected Papers of E. M. Lifshitz*, edited by L. P. Pitaevski (Pergamon Press, Oxford, 1992), pp. 203–218.